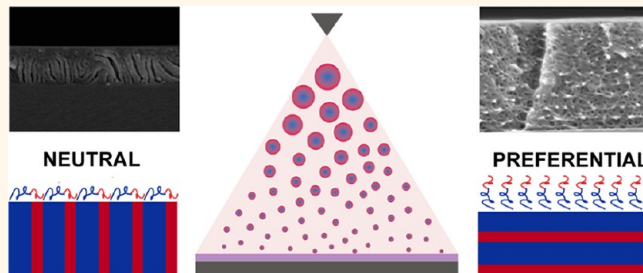


# Continuous Equilibrated Growth of Ordered Block Copolymer Thin Films by Electrospray Deposition

Hanqiong Hu,<sup>†</sup> Sofia Rangou,<sup>‡,§</sup> Myungwoong Kim,<sup>†</sup> Padma Gopalan,<sup>†</sup> Volkan Filiz,<sup>§</sup> Apostolos Avgeropoulos,<sup>‡</sup> and Chinedum O. Osuji<sup>†,\*</sup>

<sup>†</sup>Department of Chemical and Environmental Engineering, Yale University, New Haven, Connecticut 06511, United States, <sup>‡</sup>Department of Materials Science and Engineering, University of Ioannina, University Campus-Dourouti, Ioannina 45110, Greece, <sup>§</sup>Helmholtz-Zentrum Geesthacht, Institute of Polymer Research, Max-Planck-Strasse 1, 21502 Geesthacht, Germany, and <sup>†</sup>Department of Materials Science and Engineering, University of Wisconsin, Madison, Wisconsin 53706, United States

**ABSTRACT** Deposition of block copolymer thin films is most often accomplished in a serial process where material is spin coated onto a substrate and subsequently annealed, either thermally or by solvent vapor, to produce a well-ordered morphology. Here we show that under appropriate conditions, well-ordered block copolymer films may be continuously grown under substrate equilibrated conditions by slow deposition of discrete subattoliter quantities of material using electrospray. We conduct time-resolved observations and investigate the effects of process parameters that underpin film morphology including solvent selectivity, substrate temperature, block-substrate selectivity, and flow rate of the feed solution. For a PEO cylinder-forming poly(styrene-*b*-ethylene oxide) block copolymer, we uncover a wide temperature window from 90 to 150 °C and an ideal flow rate of 2  $\mu$ L/min for ordered film deposition from dilute acetone solutions. PEO cylinders aligned with their long axes perpendicular to the film–air interface at optimal spray conditions. Using poly(styrene-*b*-methyl methacrylate) deposited onto neutrally selective surfaces, we show that the substrate-equilibrated process results in vertically oriented microdomains throughout the film, indicating a preservation of the initial substrate-dictated morphology during the film deposition. Electrospray offers a new and potentially exciting route for controlled, continuous growth of block copolymer thin films and manipulation of their microstructure.



**KEYWORDS:** block copolymer · thin films · electrospray · film growth · self-assembly

Block copolymers have demonstrated great potential as functional thin films, with their function strongly linked to their mesoscale self-assembly. Spin-coating and solvent vapor annealing have been used extensively to prepare well-ordered block copolymer thin films *via* solvent mediation of substrate affinity and block interactions. The resulting film morphology is dictated by a complex interplay of surface energies (substrate and free-air interface), polymer–solvent interactions, and the commensurability between the film thickness and half or whole-integer multiples of the microdomain spacing.<sup>1</sup> In many situations, such as in pattern transfer lithography<sup>2–5</sup> and selective transport membranes,<sup>6–13</sup> the desired outcome is the production of vertically aligned lamellar

or cylindrical microdomains or microstructures in thin films ranging from 0.1 to 10  $\mu$ m in thickness. For very thin films (*ca.* 100 nm or less), this can be achieved with high fidelity by tailoring the substrate to display a neutral wetting condition<sup>14–16</sup> with respect to the polymer blocks, and, optionally, by managing the polymer–solvent interactions at the air interface to promote the presence of both blocks at the free surface.<sup>17–19</sup> Unfortunately, this approach is not viable for thicker films as the influence of the neutral substrate generally does not persist beyond *ca.* 100 nm<sup>20–22</sup> without the aid of either small molecule surfactant additives<sup>23</sup> or the use of significantly higher annealing temperatures.<sup>22</sup> A further drawback is the fact that 80–90% of dispensed material is wasted or goes unrecovered in

\* Address correspondence to chinedum.osuji@yale.edu.

Received for review May 15, 2012 and accepted March 3, 2013.

Published online March 04, 2013  
10.1021/nn400279a

© 2013 American Chemical Society

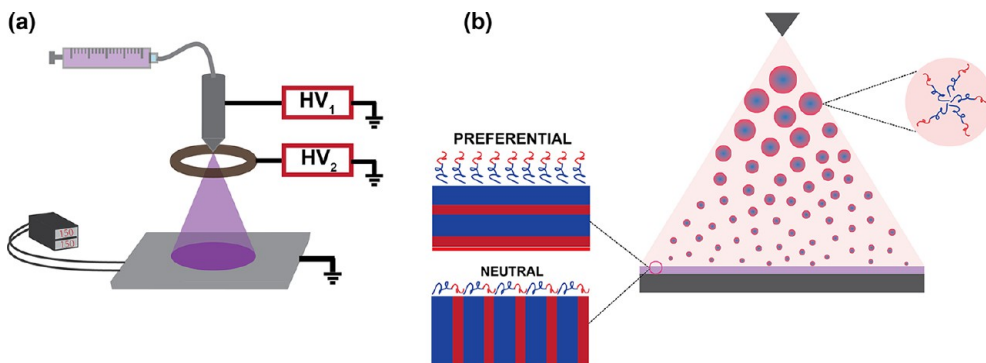


Figure 1. (a) Schematics of electrospray setup. (b) Slow block copolymer deposition via electrospray generated droplets and equilibration in the presence of existing deposited material. A neutral surface promotes vertical growth of the microstructure while a preferential surface generates planar orientation. Micelles and/or dissolved chains of the block copolymer exist within each droplet.

typical spin-coating operations. We are thus motivated to develop new approaches that permit the deposition of ordered block copolymer films of arbitrary thickness, ideally, in a continuous fashion, while avoiding the waste of potentially expensive materials.

Effectively, we seek to mimic the targeted vapor deposition processes that are used to grow well-ordered inorganic thin films which, optionally, may also involve epitaxy between the deposited material and the substrate. With few exceptions however, macromolecules are not amenable to vapor delivery. We propose instead to achieve the required slow delivery of polymer chains to a substrate by using electrospray atomization<sup>24–27</sup> of dilute solutions such that, on average, each arriving droplet delivers no more than *ca.* 100 nm-thickness worth of polymer. The equilibration of this sub-100 nm material on the substrate then occurs subject to the relevant wetting condition presented by the substrate or previously deposited material. Further, the droplet should be sufficiently small such that the solvent does not perturb the surface, for example, by cratering, by more than *ca.* 100 nm. The size of the droplet is dictated by the conditions of the electrospray and any loss of solvent by evaporation in flight to the substrate. Finally, the rate of droplet arrival must be less than the rate of equilibration of deposited material so that films grow while in constant thermal equilibrium with the substrate.

The concept is illustrated schematically in Figure 1a, which shows an electrospray setup with an extractor ring and temperature control of the grounded substrate. Electrospray is well established as a method for the preparation of droplets of various sizes ranging from molecular dimensions to hundreds of micrometers, as well reviewed.<sup>26,28,29</sup> A liquid solution becomes charged as it is fed through a capillary connected to a high voltage power supply. On exiting the capillary, the fluid elongates into a jet under the influence of the electric field-induced shear stress on the liquid surfaces. In the cone-jet mode, the charged

liquid surface takes a conical shape, referred to as a Taylor cone. The liquid jet breaks up into droplets away from the cone tip carrying a charge close to the Rayleigh limit. Studies have established scaling rules which describe the dependence of droplet size  $d$  on flow rate, applied voltage, and liquid conductivity as shown in eq 1<sup>30</sup>

$$d = \alpha \left( \frac{Q^3 \varepsilon \rho}{\pi^4 \sigma \gamma} \right)^{1/6} \quad (1)$$

where  $\alpha$  is a constant depending on the fluid's dielectric permittivity,  $Q$  is the flow rate,  $\varepsilon$  is the dielectric constant,  $\rho$  is the density,  $\sigma$  is the surface tension, and  $\gamma$  is the conductivity of the liquid. In the cone-jet mode, narrow droplet size distributions with standard deviations from 5 to 15% are typical.<sup>31,32</sup> The viscosity of polymer solutions at elevated concentrations results in fiber formation instead of droplet breakup, that is, electrospinning. Figure 1b describes the deposition and ordering of the film. Solvent evaporates leading to increasing polymer concentration within the droplets as they travel toward the substrate under the electric field stabilized by the extractor ring. Once the material arrives at the substrate, it relaxes and equilibrates at the prescribed temperature with any material already present on the substrate.

Here, we introduce electrospray as an effective means of depositing well-ordered block copolymer thin films in such a continuous or uninterrupted fashion, as described above. Despite the clear potential as framed in the discussion above, electrospray has been applied to polymer deposition only to a limited extent in the production of ferroelectric PVDF materials, with a strong emphasis on controlling film roughness and crystal form as recently reported.<sup>33–35</sup> Somewhat surprisingly, to the best of our knowledge, electrospray has not previously been applied to controlled growth of block copolymer thin films. This is all the more striking given the prevalence of electrospinning of block copolymers and polymer nanocomposites.<sup>36–38</sup>

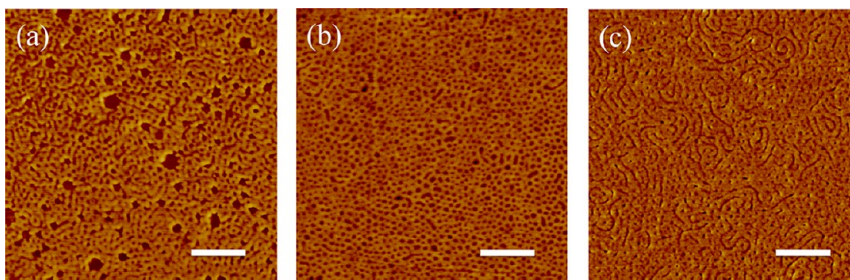


**Figure 2.** Plan-view AFM phase contrast images of PS-*b*-PEO films produced by 30 min of electrospray deposition at a flow rate of 2  $\mu$ L/min and substrate temperature of 150  $^{\circ}$ C from 0.03 wt % solutions in (a) THF; (b) acetone; (c) acetonitrile. Scale bar: 400 nm.

We study the deposition of cylinder-forming poly(styrene-*b*-ethylene oxide), PS-*b*-PEO, and highlight the optimal conditions for film growth. We show that the film growth is linear in time and that the system can be biased to produce vertically oriented microdomains at the free air interface. Using a cylinder-forming poly(styrene-*b*-methyl methacrylate), PS-*b*-PMMA, we show that a well engineered neutral wetting surface enables the continuous growth of vertically oriented domains throughout the film. This has potential broad utility in applications reliant on deposition of well-ordered block copolymer thin films and likely other materials as well.

## RESULTS AND DISCUSSION

**Solvent Selectivity.** We investigated the role of solvent selectivity using PS-*b*-PEO by electrospraying for 30 min from THF, acetone, and acetonitrile solutions at a fixed flow rate of 2  $\mu$ L/min. At this flow rate, films grew to a thickness of 115 nm during the deposition, implying a slow growth rate of approximately 4 nm/min. The substrate temperature was held constant at 150  $^{\circ}$ C. In all cases, the obtained films were macroscopically smooth, with RMS roughnesses less than 3 nm. We obtained morphologies by AFM as shown in Figure 2. The primary difference across the solvents was in the propensity of the cylindrical PEO microdomains to adopt a vertical orientation at the free air surface. Acetone produced almost uniform perpendicular or vertically aligned microdomains, whereas acetonitrile derived films had a mixture of perpendicular and parallel cylinders. Films produced from THF showed a majority of perpendicular microdomains mixed with a minority of short parallel-oriented cylinders. Additionally, we observed several 100–300 nm diameter circular features in the film, the origins of which are unclear. One possibility is that they are produced by arrested dewetting of the film. It is more likely that they are due to trace impurities often encountered with THF—either oxidative peroxide products, or the butylated hydroxytoluene stabilizers meant to inhibit peroxide formation.

It is notable that in all cases discussed here, the deposited films exhibited excellent smoothness, with RMS roughness similar to or less than 3 nm. This is

remarkable as one of the principal challenges in the deposition of high quality polymer films by electrospray is in fact the suppression of film roughness, with reported RMS roughnesses of several tens of nanometers not atypical for films varying from 100 to 400 nm.<sup>39</sup> The film roughness is impacted by a number of parameters and it is generally difficult to attribute smoothness or lack thereof to a single experimental parameter.<sup>35</sup> We can say anecdotally however that films sprayed from lower volatility and lower conductivity solvents such as toluene or benzene generally exhibited greater roughness.

Since it is not cross-linked, the adhesion layer is free to undergo reorganization by thermal annealing during the film deposition. As such we do not expect an epitaxial growth in which the film replicates the features of the adhesion layer; that is, the layer functions only to promote adhesion and not to guide the morphology of deposited material, as corroborated by control experiments using PS homopolymer and silane adhesion layers (Supporting Information Figure S12). The deviation of the morphologies (Figure 2) from those presented by the adhesion layer (Figure S11b) substantiates this and indicates instead that the solvent-mediated film–air interface dictates the morphology of freshly deposited material. We expect that solvent selectivity can modify the preference of the PS and PEO blocks for the interfaces, and in particular, reduce the segregation of the lower surface energy block to the air interface. Given the solubility parameters ( $\delta_{\text{THF}} = 9.1$ ,  $\delta_{\text{acetone}} = 9.9$ ,  $\delta_{\text{acetonitrile}} = 11.9$ ,  $\delta_{\text{PS}} = 8.7$ ,  $\delta_{\text{PEO}} = 10.5$  (cal/cm<sup>3</sup>)<sup>1/2</sup>), THF is selective for PS, acetone is selective for PEO, and acetonitrile is very selective for PEO. The selectivity of acetone for PEO likely offsets the preference of PS for the film–air interface, thus favoring a perpendicular orientation. Directional evaporation of any residual solvent from the film can also influence the equilibration dynamics and contribute to perpendicular morphology.<sup>40,41</sup> Interfacial preference as well as block interactions can also be readily tuned through the addition to the solution of species such as inorganic salts which selectively sequester into or associate with one block.<sup>42–45</sup> Here, for acetonitrile solutions, we observe that the addition of small

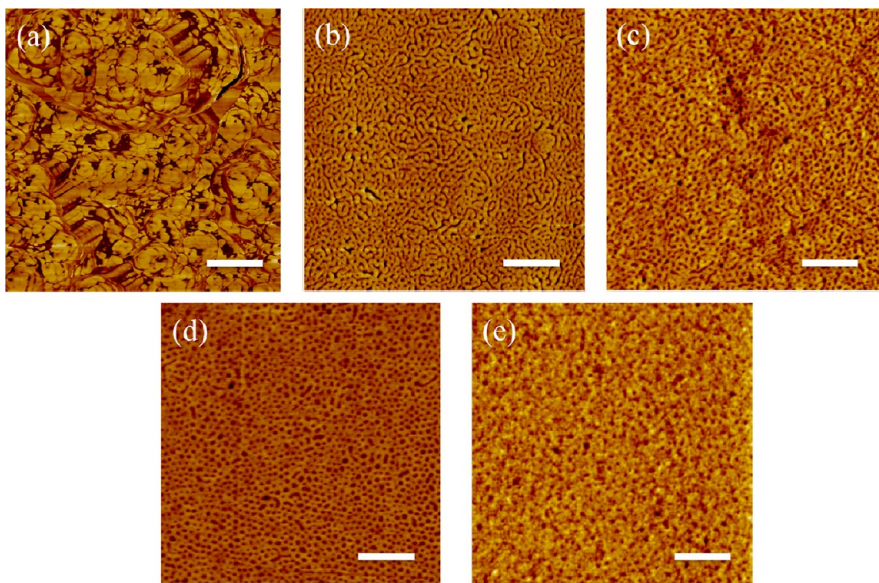


**Figure 3.** Plan-view AFM phase contrast images of electrosprayed PS-*b*-PEO films from 0.03% acetone solution at flow rate of 2  $\mu$ L/min for 30 min at different substrate temperatures: (a) 60, (b) 90, (c) 120, (d) 150, and (e) 180  $^{\circ}$ C. Scale bar: 400 nm.

amounts of a gold salt, chloroauric acid, results in a transformation from mixed parallel and perpendicular to exclusively perpendicular cylindrical microdomains (Supporting Information, Figure SI3).

**Deposition Temperature.** As described earlier, the kinetic balance between relaxation and deposition of the material is expected to underpin the development of ordered morphologies in the electrosprayed films. For a given rate of deposition determined by the feed solution flow rate, the relaxation or equilibration of deposited material will be governed by the diffusivity of the polymer in the film. This in turn is controlled principally by the substrate temperature. The dependence of film morphology on substrate temperature is shown by the data of Figure 3. At the lowest temperature studied, 60  $^{\circ}$ C, the films appear completely disordered in AFM and are visibly cloudy to the naked eye. It is apparent that no significant relaxation of the deposited material takes place at this temperature which is well below the glass transition temperature of PS, roughly 105  $^{\circ}$ C. The glass transition temperature of PEO is well below room temperature and so does not play a role in dictating the equilibration dynamics here. At the highest temperature, 180  $^{\circ}$ C, we find that while the polymer is clearly microphase separated, the morphology is not as well ordered as that produced at lower temperatures. This may be due to partial thermal degradation of the material as the deposition is carried out in ambient air.

Our result suggests a usable temperature window for producing ordered structures from 90 to 150  $^{\circ}$ C for the flow rate and solution concentration considered here. The fact that the system is fairly well ordered at 90  $^{\circ}$ C, below the glass transition of the PS matrix, suggests that residual solvent in the film may play a

role in the ordering process as this would decrease the effective  $T_g$  of the PS and permit chain relaxation and structure development. Further, there is a clear transition from mixed parallel/perpendicular to exclusively perpendicular cylinders at temperatures above 90  $^{\circ}$ C. We conclude that 150  $^{\circ}$ C is an optimal substrate temperature for this system. It permits sufficient mobility to produce well-ordered films and yields a perpendicular morphology.

**Feed Solution Flow Rate.** The effect of feed solution flow rate on electrospray deposition can be understood in terms of the resulting mean droplet size and film deposition rates. The conceptual starting point for continuous growth of ordered thin films was that each arriving droplet delivered no more than *ca.* 100 nm thickness-worth of material. We examined this by characterizing the size of individually deposited polymer particles. From this we can deduce the initial size of the droplets produced by the spray conditions using the known concentration of the polymer in solution. Figure 4 demonstrates the effect of solution flow rate on film morphology, with 2, 4, 8, and 16  $\mu$ L/min flow rates sampled. Flow rates beyond 16  $\mu$ L/min could not be reliably considered due to the instability of the Taylor cone observed in this regime. The deposited films were well ordered in all four cases with only slight variations of PEO cylinder orientations. However, the roughness of the films increased sharply with the increase of flow rate as reflected by the increasing heterogeneity in optical micrographs taken at increasing flow rates, Figure 4e–h.

Brief depositions (5–10 s) were performed to produce very low coverage films. This permitted imaging the material deposits delivered by individual droplets, as typically done in *posteriori* characterization of

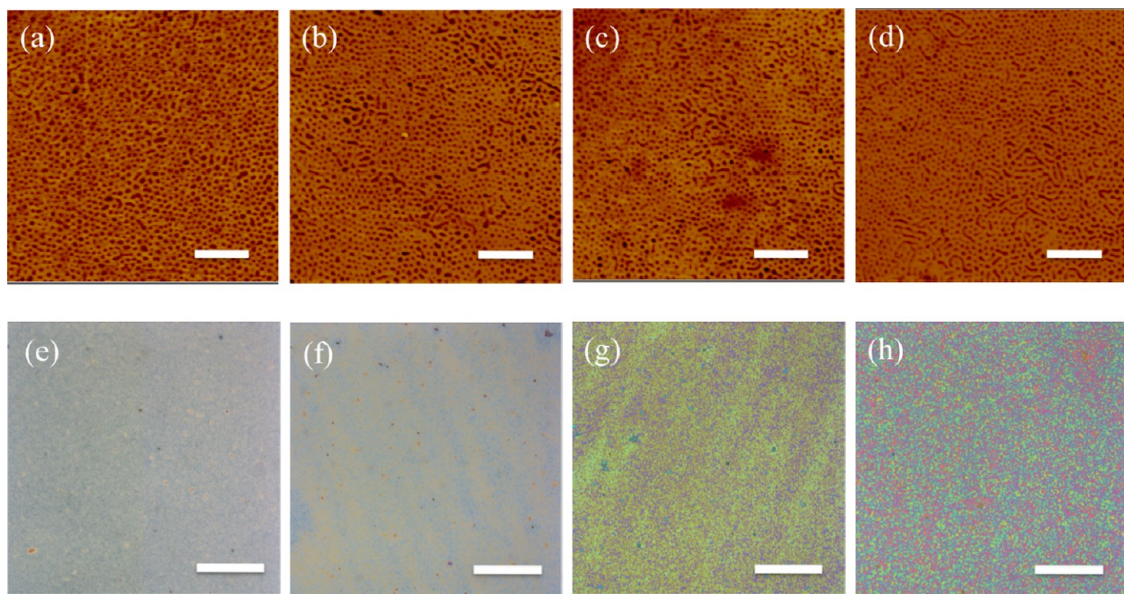


Figure 4. Plan-view AFM phase images (top) and optical graphs (bottom) of PS-*b*-PEO films electrosprayed from 0.03% acetone solution at different flow rates: (a, e) 2, (b, f) 4, (c, g) 8, (d, h) 16  $\mu$ L/min. Scale bar: top, 400 nm; bottom, 90  $\mu$ m.

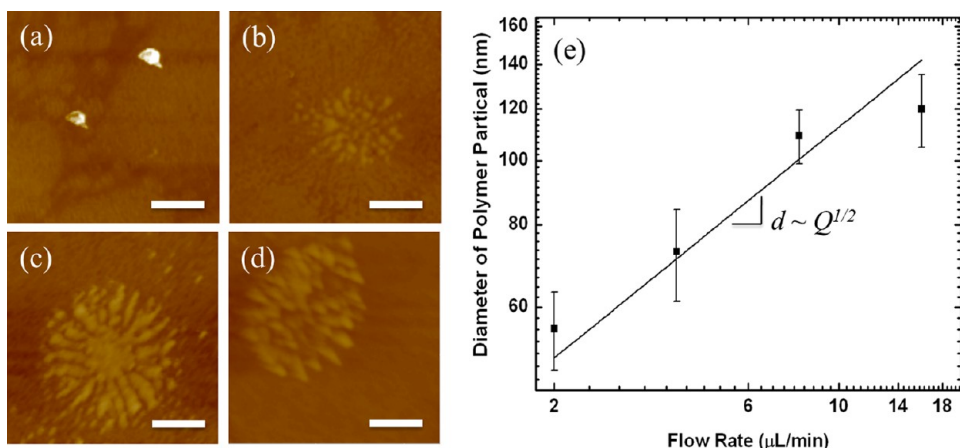


Figure 5. AFM height images (full-scale intensity corresponds to 20 nm) of material deposited from 0.03% acetone solution at (a) 2, (b) 4, (c) 8, (d) 16  $\mu$ L/min. Scale bar: 400 nm. The thicknesses of the deposited material inferred at each flow rate are 7.6, 1.9, 3.4, and 2.6 nm, respectively. (e): Calculated polymer particle size as a function of flow rate. The line fits the data to a square-root dependence as a guide to the eye.

droplet size distributions in electrospray.<sup>46,47</sup> The volume of individual deposits was determined from AFM height images and the droplet size was represented as the diameter of a sphere of the same volume. The results are shown in Figure 5. The AFM images indicate that significant flattening of deposited material occurs for all flow rates, with the greatest flattening at the highest flow rates. Higher flow rates clearly result in enough retention of solvent to produce roughly micrometer-scale splash patterns on the substrate.

The implication here is that changing the flow rate affects not only the overall deposition rate, but may also significantly affect the subsequent equilibration of the film through the delivery of residual solvent. The dryness of the deposited material therefore should be considered in addition to the other process parameters

outlined thus far. The solvent content is a nontrivial function of the ambient air temperature, initial droplet size, solvent vapor pressure, and even substrate temperature, *via* the convective heat transfer near the surface. While the presence of residual solvent represents a departure in principle from the analogy constructed with vapor deposition processes earlier, it represents an important handle with which one can tune the resulting film morphology. The effective diameter of individual material deposits exhibited slightly more than a 2-fold increase, ranging roughly from 55 to 120 nm. This agrees reasonably well with calculations given the 8-fold increase in the flow rate from 2 to 16  $\mu$ L/min and the quadratic dependence of volume on particle diameter in eq 1. The dimensions here correspond to initial droplet sizes ranging from

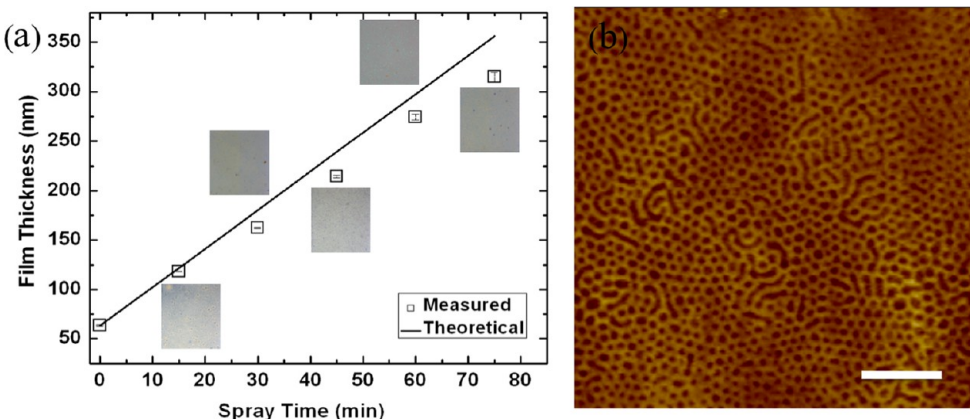


Figure 6. (a) Electrosprayed PS-*b*-PEO film thickness as a function of spray time. Inset: optical micrographs ( $360 \times 360 \mu\text{m}^2$ ) at each time point. (b) AFM phase image of electrosprayed PS-*b*-PEO from 0.03 wt % acetone solution at flow rate of  $2 \mu\text{L}/\text{min}$  for 150 min. Scale bar: 400 nm.

900 to 1650 nm. We conclude that for the current setup,  $2 \mu\text{L}/\text{min}$  represents the optimal flow rate of those considered. It provides the least susceptibility to the particular ambient conditions present during deposition given that it results in the delivery of material with the least amount of residual solvent. A more detailed study on the impact of ambient conditions on film morphology is needed and will be pursued in future work.

**Time-Resolved Evolution of Film Morphology.** To verify the utility of the electrospray process for continuous deposition, we examined the time-resolved production of films under the optimal conditions identified,  $2 \mu\text{L}/\text{min}$ ,  $150^\circ\text{C}$ , 0.03 wt % acetone feed solution. As shown in Figure 6a, film thickness was measured at 15-min intervals during deposition on a single sample, for 75 min. The sample was removed from the spray, characterized by ellipsometry, and then returned to the apparatus for additional deposition. The spray time shown in the plot is therefore the cumulative spray time for the sample. A simple calculation based on the known polymer concentration, solution flow rate, and deposited area suggests a film growth rate of  $3.9 \text{ nm}/\text{min}$  or  $58.5 \text{ nm}$  per 15 min interval. The measured film thicknesses are in very good agreement with the calculation but exhibit a small disparity that likely results from inadvertent loss of material during flight to the substrate and potentially uneven distribution of material within the deposited area. Optical micrographs (insets of Figure 6a) of the film at each time point confirm that the film is macroscopically smooth. In a separate experiment, deposition was conducted uninterrupted for 150 min, producing a  $0.6 \mu\text{m}$  thick film with a well ordered morphology as shown in Figure 6b. The main impediment to continuous unaided deposition is the potential for loss of stability of the Taylor cone due to perturbations of the sample environment. The process can be stabilized for long-term depositions by building an environmental chamber to prevent convective currents and transients

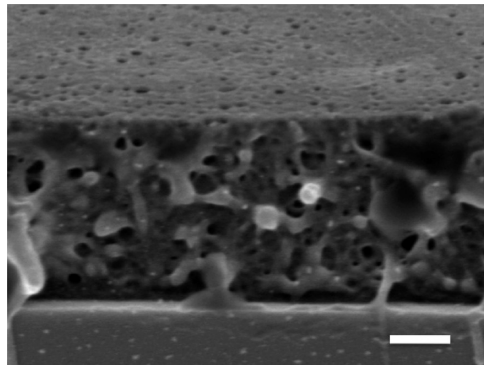
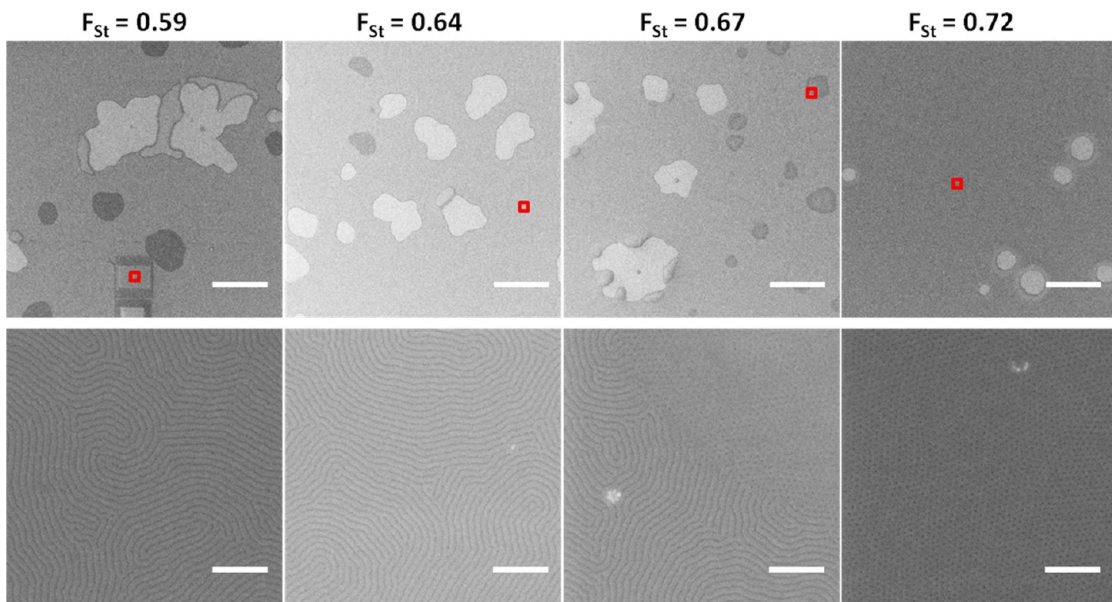


Figure 7. Cross-sectional view of PS-*b*-PEO films showing parallel cylinders in the interior of the film, but perpendicular cylinders in the near surface region. The sample shows some distortion that occurred during fracture. Scale bar: 200 nm.

in ambient temperature and relative humidity. The use of higher conductivity solutions can also help to stabilize the spray.

The consistent observation of perpendicularly oriented cylinders at the film surface at each point in the time-resolved experiment (Supporting Information Figure S14a-e) suggests that the microdomains may be vertically continuous throughout the film depth. Cross-sectional examination however shows that this is not the case. The vertical microstructure persists into the film for a few tens of nanometers before giving way to a parallel orientation of the PEO microdomains, Figure 7. This result is quite striking. It indicates that the morphology of freshly deposited material is dictated by the solvent–air interface initially, but this vertically aligned cylinder morphology relaxes as the sample is annealed. This equilibration results in adoption of the parallel arrangement at long times as newly deposited material becomes buried. It is well-known that freshly cleaned silicon surfaces with their native oxide are preferential for PEO over PS, resulting in parallel alignment of microdomains.<sup>48,49</sup> It is apparent here that the silicon substrate imposes this preferential wetting



**Figure 8.** Plan-view SEM images of PS-*b*-PMMA spin coated and annealed on P(S-*r*-MMA-*r*-GMA) wetting layers with compositions,  $F_{st}$ , as indicated. Top row: Low magnification; scale bars,  $10\ \mu\text{m}$ . Bottom row: High magnification data taken within the square regions indicated in the low magnification images. Scale bars:  $300\ \text{nm}$ .

condition and that it acts throughout the deposition, resulting in the parallel oriented morphology as the film equilibrates continuously with the substrate.

The persistence of the substrate-dictated parallel morphology in the PS-*b*-PEO case suggests that vertically oriented microdomains may be produced throughout a deposited film if the substrate wetting condition favors such vertical alignment initially. For this purpose we leveraged the well developed PS-*b*-PMMA system in which modification of the substrate by the appropriate P(S-*r*-MMA) copolymer leads to vertically oriented morphology in sub-100 nm films.<sup>14,16,22,50</sup> In this case, the copolymer contains a small fraction ( $\sim 4$  mol %) of glycidyl methacrylate which permits cross-linking of the wetting layer. It is known from previous studies that there is a compositional window of the copolymer which results in a nonpreferential surface for PS-*b*-PMMA.<sup>16,51</sup> For the assembly of PS-*b*-PMMA in this study four random copolymers with a styrene mole fraction ( $F_{st}$ ) ranging from 0.6 to 0.72 were synthesized. A 25 nm film of PS-*b*-PMMA was deposited by spin coating onto the copolymer wetting layer and was annealed under vacuum for 3 h at  $220\ ^\circ\text{C}$ . On the basis of the analysis of the top down SEM of the assembled BCP (Figure 8), an optimum composition of  $F_{st}$  of 0.72 was chosen to be the neutral surface.

A random copolymer with  $F_{st} = 0.72$  was therefore used to create the neutral wetting layer for the subsequent electrospray experiments. The data are shown in Figure 9. The samples suffered some distortion during fracture and during the swelling/deswelling technique used to improve contrast, with matrix collapse visible in some areas. Nonetheless, the essential

features are evident. Films were deposited at growth rates from 1 to 2 nm/min at temperatures between  $190$  and  $200\ ^\circ\text{C}$  from either acetone or 1:1 mixtures of acetone and chloroform, which demonstrated similar results. Under these optimal conditions, vertically aligned PMMA cylinders were produced, over a range of film thickness, up to roughly 500 nm. The use of much faster growth rates, 8–12 nm/min resulted in the loss of the vertical continuity of the PMMA microdomains, Figure 9d, implying that the deposition was no longer taking place under continuous equilibration with the substrate. Deposition in the absence of the neutral wetting layer produces parallel alignment of the PMMA cylinders within the bulk, although at the film–air interface the orientation was vertical, likely due to solvent-mediation of the interaction coupled with effects from evaporation of any residual solvent (Supporting Information Figure S15), as also observed with PS-*b*-PEO.

With conventional spin-coating and thermal annealing on a neutral wetting layer, the film thickness over which vertical alignment is preserved is less than 100 nm, and more commonly in the 50 nm range for the 50–100K molecular weight PS-*b*-PMMA typically employed, as highlighted by Ham *et al.*<sup>52</sup> Recent work has shown that prolonged annealing at high temperatures (1 day,  $230\ ^\circ\text{C}$ ) can extend this thickness range to some 900 nm with the high temperature acting effectively to suppress the surface tension differences between PS and PMMA.<sup>22</sup> In the approach presented here, the solvent vapor plays this role instead and enables film deposition under less aggressive conditions. Compellingly, as a continuous process, the only limitation on the film thickness in principle is the

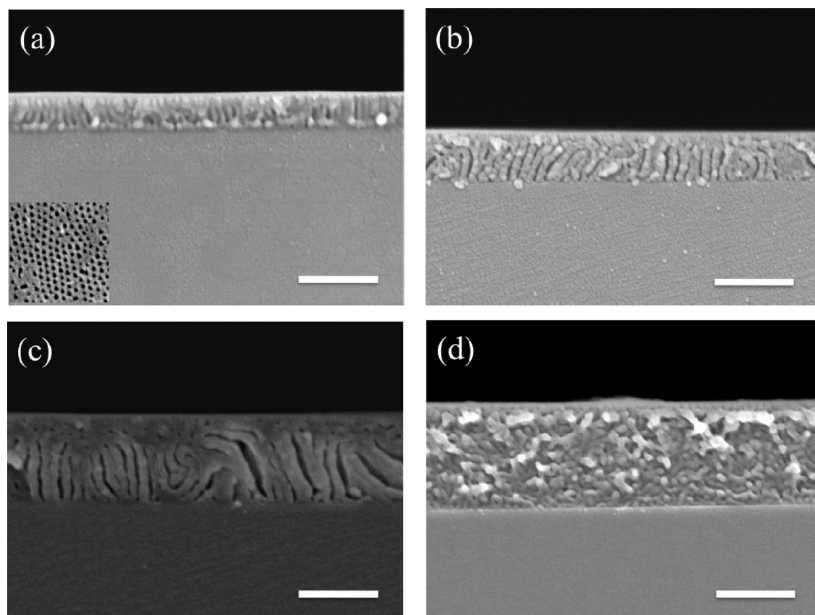


**Figure 9.** Cross-sectional views of PS-*b*-PMMA films of varying thicknesses deposited onto neutral wetting layers at low growth rates of 1–2 nm/min showing vertically oriented PMMA cylinders: (a) 170 nm; inset shows the plan-view of the film (500 nm  $\times$  500 nm); (b) 275 nm; (c) 460 nm; (d) PS-*b*-PMMA deposited at very high growth rates of 8–12 nm/min. All scale bars: 400 nm.

deposition time. Where careful control of the substrate provides a neutral wetting condition, vertical alignment of microdomains can be achieved. Alternatively, preferential wetting produces parallel morphologies. Further highlighting this last point, a lamellar forming PS-*b*-P4VP block copolymer deposited onto wafers modified with cross-linked P4VP thin layers resulted in parallel lamellae due to the strong preference of P4VP block for the substrate (Supporting Information Figure S16). The parallel orientation was maintained over all thicknesses considered, up to 2  $\mu$ m.

## CONCLUSION

We have demonstrated that electrospray atomization of dilute polymer solutions can be used as a novel and flexible tool for the continuous deposition of ordered block copolymer thin films. Cylinder-forming PS-*b*-PEO and PS-*b*-PMMA were deposited continuously yielding ordered films with thicknesses over 500 nm. The use of neutral wetting substrates in PS-*b*-PMMA resulted in the growth of vertically oriented PMMA cylindrical microdomains during the deposition. Parametric studies conducted with PS-*b*-PEO show that solvent selectivity plays an important role in determining the film morphology as it mediates the preference of the blocks for the free air interface. This is

somewhat akin to the means by which solvent vapor annealing can result in either parallel or perpendicular morphologies at the surface of block copolymer films. The development of well phase separated microstructures is predicated on rapid relaxation or equilibration of deposited material relative to the rate of overall deposition. This is largely dictated by the substrate temperature and the feed solution flow rate, respectively. We observed a wide temperature window of 90 to 150 °C and flow rate range from 2  $\mu$ L/min to 16  $\mu$ L/min that resulted in well formed microstructures in the deposited films. The presence of residual solvent within arriving material at higher flow rates can change the deposition mode from “dry” to “wet”. With the assistance of such residual solvent, larger droplets generated at higher flow rates may also relax sufficiently quickly to compensate for the higher deposition rate without compromising the morphology of the film. The relative ease with which the spray parameters can be tuned suggests that electrospray may offer a versatile approach for continuous deposition or “growth” of block copolymer thin films, conceivably with reliability over the orientation of the microstructure, as mediated by solvent evaporation and other factors. Such a development would be broadly enabling for thin film applications of block copolymers.

## MATERIALS AND METHODS

**Materials.** Poly(styrene)-*b*-poly(ethylene oxide), PS-*b*-PEO, was synthesized by sequential anionic polymerization as previously described.<sup>53,54</sup> Briefly, the polymerization of styrene was initiated by sec-BuLi in the presence of the phosphazene base

(P<sub>4</sub>tBu) at –70 °C and the reaction was left under stirring for 2 h at these conditions. Ethylene oxide was condensed in the reactor, after purification, and the solution was stirred for 30 min at –30 °C. The temperature of the solution was gradually increased to 40 °C and then the polymerization was left until

completion for 3 days. The polymerization was terminated by the addition of 1% solution of acetic acid in methanol. After removal of THF under reduced pressure, the polymer was precipitated in hexane. The composition of the block copolymer was determined by <sup>1</sup>H NMR spectroscopy. All proton nuclear magnetic resonance (<sup>1</sup>H NMR) measurements were performed on a Bruker Advance 300 NMR spectrometer at 300 MHz with internal standard (tetramethylsilane (TMS)) using chloroform (CDCl<sub>3</sub>) as the solvent. Molecular weights and polydispersities were determined by gel permeation chromatography (GPC) and the measurements were performed at 50 °C in dimethylacetamide (DMAC) using 3  $\mu$ m PSS SDV gel columns at a flow rate of 1.0 mL/min (VWR-Hitachi 2130 pump). A Waters 2410 refractive index detector ( $\lambda = 930$  nm) using a polystyrene calibration curve was used.

The molecular weight of the PS-*b*-PEO copolymer is 66 kg/mol with 47 kg/mol PS and 19 kg/mol PEO. The volume ratio of PEO is 0.27 given the bulk density of 1.05 g/cm<sup>3</sup> for PS and 1.13 g/cm<sup>3</sup> for PEO. Small angle X-ray scattering (SAXS) experiments were carried out to study the morphology of the material using a Rigaku S-3000 system with Cu K $\alpha$  source at a wavelength of  $\lambda = 1.5405$  Å. The bulk material microphase separates into hexagonally packed cylinders indicated from the SAXS data for as-cast films (Supporting Information, Figure SI1a). The primary scattering peak is at  $q = 0.151$  nm<sup>-1</sup> corresponding to a *d*-spacing of 41.6 nm. From the volume ratio, we can further deduce that the diameter of PEO cylinders is 26.3 nm with a center–center spacing of 47.9 nm.

Poly(styrene-*b*-methyl methacrylate) was purchased from Polymer Source with a molecular weight of 73.5 kg/mol and a PMMA weight fraction of 0.28. The system forms PMMA cylinders with a *d*-spacing of approximately 44 nm. A random copolymer poly(styrene-*r*-methyl methacrylate-*r*-glycidyl methacrylate), P(S-*r*-MMA-*r*-GMA) was synthesized as described previously<sup>51</sup> with four weight fractions of PS varying from 0.6 to 0.72. The composition ( $F_{S_r}$ ) of random copolymers was determined by <sup>1</sup>H NMR spectroscopy.

**Substrate Modification.** Dewetting of PS-*b*-PEO was sometimes encountered on bare silicon wafers, particularly during long depositions at higher temperatures. In such cases it was observed that the presence of an initially spin-coated layer of material served to inhibit dewetting, apparently by promoting adhesion of the deposited material to the substrate. PS homopolymer, silane monolayers as well as the PS-*b*-PEO block copolymer itself were all found to function satisfactorily and equally in this regard, with no resulting difference in film morphology, as described in the Supporting Information (Figure SI2). The use of PS-*b*-PEO for the adhesion layer was adopted as the standard protocol for these studies. The adhesion layer was deposited by spin-coating PS-*b*-PEO onto 1 cm × 1 cm piranha-cleaned silicon wafer chips using a 1 wt % benzene solution. The resulting film has a thickness around 55 nm as determined by ellipsometry, with PEO cylinders oriented parallel to the substrate (Supporting Information, Figure SI1b). For PS-*b*-PMMA, substrate modification to produce a neutral wetting surface was accomplished as previously described.<sup>51</sup> This involved depositing P(S-*r*-MMA-*r*-GMA) by spin coating from 0.3 wt % toluene solution, followed by annealing under vacuum at 160 °C for 3 h to cross-link the films. Substrates were rinsed in toluene prior to use to remove any excess noncross-linked material.

**Electrospray Deposition of Block Copolymer Thin Films.** Dilute solutions of 0.03 wt % PS-*b*-PEO in acetone, tetrahydrofuran (THF), and acetonitrile were prepared and filtered using 0.2  $\mu$ m PTFE filters. For PS-*b*-PMMA, solutions of the same concentration were prepared in like manner in acetone or a 1:1 mixture of acetone and chloroform. The spray setup is shown in Figure 1a. The capillary used in the study is a 36 gauge blunt stainless steel needle (NanoFil, World Precision Instruments) with inner diameter of 35  $\mu$ m and outer diameter of 110  $\mu$ m. A homemade brass extractor ring was used to enhance the stability of the spray. It was placed concentrically about 1 mm below the needle tip. Both the needle tip and ring were maintained at 4 and 2.3 kV, respectively, using commercial HV sources (EMCO and Acopian).

Block copolymer solutions were fed into the needle using a programmable syringe pump at different flow rates from 2 to 16  $\mu$ L/min. The droplets were collected on silicon substrates placed on a temperature controlled ground plate approximately 3 and 5 cm (in the case of some lower deposition rate experiments with PS-*b*-PMMA) from the needle exit. The substrates were preheated for 20 s on the ground plate and then quickly slid into the spray for a given period of time. After deposition, samples were kept outside of the spray on the heated plate for 30 s to ensure removal of any residual solvent in the films and then stored under vacuum for later characterization. It should be noted that the quality of the film is predominantly dictated by the quality and stability of the spray. In all experiments, the system was monitored visually using a magnifying eyepiece to ensure that the Taylor cone was stable and fluid-filled. Additionally, two multimeters were incorporated into the apparatus to monitor the needle-extractor and extractor-substrate currents. The relative magnitude of these two currents is related to the ratio of substrate-deposited to extractor-deposited material.<sup>55,56</sup> In all cases, we confirmed that the measured current was stable and that no significant needle-extractor current flows were present, indicating that the cone-jet mode was stable.

**Characterization of Deposited Films.** The thickness of deposited films was characterized by single wavelength ellipsometry ( $\lambda = 632.8$  nm) (Angstrom Advanced, Inc.) at an incident angle of 65°. Data were simulated using commercial software (Phe-101, Angstrom Advanced, Inc.). Optical textures of the films were recorded in reflection on a Zeiss Axiovert 200 M optical microscope. Atomic Force Microscopy (AFM) was performed using a Multimode AFM with a Nanoscope IIIa controller (Veeco) under tapping mode. Films were imaged using a Hitachi SU-70 SEM at an accelerating voltage of 2 kV. Samples were momentarily dipped in a minority phase selective solvent such that the rapid swelling and deswelling of the microdomains served to enhance the contrast under secondary electron detection. Ethanol and a 60/40 mixture of isopropyl alcohol/water were used for PS-*b*-PEO and PS-*b*-PMMA, respectively. For cross-sectional microscopy, samples were fractured under liquid nitrogen after notching the silicon wafer to produce a clean edge for imaging.

**Conflict of Interest:** The authors declare no competing financial interest.

**Acknowledgment.** The authors are grateful to Alessandro Gomez and Begona Almeria for helpful discussions and critical insight in the development of the electrospray procedures. The authors thank the referees for particularly helpful feedback during the review process. C.O. and H.H. acknowledge financial support by NSF through DMR-0847534 and DMR-0934520. Facilities use was supported by YINQE and NSF MRSEC DMR-1119826. P.G. acknowledges partial financial support from the National Science Foundation-Nanoscale Science and Engineering Center at the University of Wisconsin-Madison (Grant No. DMR-0832760) and from the Wisconsin Alumni Research Foundation. P.G. and M.K. acknowledge support from the staff and the use of equipment at the Materials Science Center and Soft Materials Laboratory at the University of Wisconsin-Madison. The authors thank Daniel P. Sweat for the synthesis of a series of P(S-*r*-MMA-*r*-GMA) copolymers.

**Supporting Information Available:** AFM and SEM micrographs of polymer films and small-angle X-ray scattering data of the bulk material. This material is available free of charge via the Internet at <http://pubs.acs.org>.

## REFERENCES AND NOTES

1. Fasolka, M. J.; Mayes, A. M. Block Copolymer Thin Films: Physics and Applications. *Annu. Rev. Mater. Res.* **2001**, *31*, 323–355.
2. Ruiz, R.; Kang, H. M.; Detcheverry, F. A.; Dobisz, E.; Kercher, D. S.; Albrecht, T. R.; de Pablo, J. J.; Nealey, P. F. Density Multiplication and Improved Lithography by Directed Block Copolymer Assembly. *Science* **2008**, *321*, 936–939.
3. Kim, S. O.; Solak, H. H.; Stoykovich, M. P.; Ferrier, N. J.; de Pablo, J. J.; Nealey, P. F. Epitaxial Self-Assembly of Block

Copolymers on Lithographically Defined Nanopatterned Substrates. *Nature* **2003**, *424*, 411–414.

- Stoykovich, M. P.; Muller, M.; Kim, S. O.; Solak, H. H.; Edwards, E. W.; de Pablo, J. J.; Nealey, P. F. Directed Assembly of Block Copolymer Blends into Nonregular Device-Oriented Structures. *Science* **2005**, *308*, 1442–1446.
- Tang, C. B.; Lennon, E. M.; Fredrickson, G. H.; Kramer, E. J.; Hawker, C. J. Evolution of Block Copolymer Lithography to Highly Ordered Square Arrays. *Science* **2008**, *322*, 429–432.
- Yang, S. Y.; Park, J.; Yoon, J.; Ree, M.; Jang, S. K.; Kim, J. K. Virus Filtration Membranes Prepared from Nanoporous Block Copolymers with Good Dimensional Stability under High Pressures and Excellent Solvent Resistance. *Adv. Funct. Mater.* **2008**, *18*, 1371–1377.
- Yang, S. Y.; Ryu, I.; Kim, H. Y.; Kim, J. K.; Jang, S. K.; Russell, T. P. Nanoporous Membranes with Ultrahigh Selectivity and Flux for the Filtration of Viruses. *Adv. Mater.* **2006**, *18*, 709–712.
- Phillip, W. A.; Dorin, R. M.; Werner, J.; Hoek, E. M. V.; Wiesner, U.; Elimelech, M. Tuning Structure and Properties of Graded Triblock Terpolymer-Based Mesoporous and Hybrid Films. *Nano Lett.* **2011**, *11*, 2892–2900.
- Drzal, P. L.; Halasa, A. F.; Kofinas, P. Microstructure Orientation and Nanoporous Gas Transport in Semicrystalline Block Copolymer Membranes. *Polymer* **2000**, *41*, 4671–4677.
- Phillip, W. A.; O'Neill, B.; Rodwgin, M.; Hillmyer, M. A.; Cussler, E. L. Self-Assembled Block Copolymer Thin Films as Water Filtration Membranes. *ACS Appl. Mater. Interfaces* **2010**, *2*, 847–853.
- Majewski, P. W.; Gopinadhan, M.; Osuji, C. O. Magnetic Field Alignment of Block Copolymers and Polymer Nanocomposites: Scalable Microstructure Control in Functional Soft Materials. *J. Polym. Sci., Part B: Polym. Phys.* **2012**, *50*, 2–8.
- Osuji, C. O. Alignment of Self-Assembled Structures in Block Copolymer Films by Solvent Vapor Permeation. *Macromolecules* **2010**, *43*, 3132–3135.
- Mauter, M. S.; Elimelech, M.; Osuji, C. O. Nanocomposites of Vertically Aligned Single-Walled Carbon Nanotubes by Magnetic Alignment and Polymerization of a Lyotropic Precursor. *ACS Nano* **2010**, *4*, 6651–6658.
- Mansky, P.; Liu, Y.; Huang, E.; Russell, T. P.; Hawker, C. J. Controlling Polymer-Surface Interactions with Random Copolymer Brushes. *Science* **1997**, *275*, 1458–1460.
- Thurn-Albrecht, T.; Steiner, R.; DeRouchey, J.; Stafford, C. M.; Huang, E.; Bal, M.; Tuominen, M.; Hawker, C. J.; Russell, T. Nanoscopic Templates from Oriented Block Copolymer Films. *Adv. Mater.* **2000**, *12*, 787–791.
- Han, E.; Stuen, K. O.; La, Y. H.; Nealey, P. F.; Gopalan, P. Effect of Composition of Substrate-Modifying Random Copolymers on the Orientation of Symmetric and Asymmetric Diblock Copolymer Domains. *Macromolecules* **2008**, *41*, 9090–9097.
- Xuan, Y.; Peng, J.; Cui, L.; Wang, H. F.; Li, B. Y.; Han, Y. C. Morphology Development of Ultrathin Symmetric Diblock Copolymer Film via Solvent Vapor Treatment. *Macromolecules* **2004**, *37*, 7301–7307.
- Peng, J.; Kim, D. H.; Knoll, W.; Xuan, Y.; Li, B. Y.; Han, Y. C. Morphologies in Solvent-Annealed Thin Films of Symmetric Diblock Copolymer. *J. Chem. Phys.* **2006**, *125*.
- Peng, J.; Xuan, Y.; Wang, H. F.; Yang, Y. M.; Li, B. Y.; Han, Y. C. Solvent-Induced Microphase Separation in Diblock Copolymer Thin Films with Reversibly Switchable Morphology. *J. Chem. Phys.* **2004**, *120*, 11163–11170.
- Mansky, P.; Russell, T. P.; Hawker, C. J.; Mays, J.; Cook, D. C.; Satija, S. K. Interfacial Segregation in Disordered Block Copolymers: Effect of Tunable Surface Potentials. *Phys. Rev. Lett.* **1997**, *79*, 237–240.
- Xu, T.; Hawker, C. J.; Russell, T. P. Interfacial Interaction Dependence of Microdomain Orientation in Diblock Copolymer Thin Films. *Macromolecules* **2005**, *38*, 2802–2805.
- Han, E.; Stuen, K. O.; Leolukman, M.; Liu, C. C.; Nealey, P. F.; Gopalan, P. Perpendicular Orientation of Domains in Cylinder-Forming Block Copolymer Thick Films by Controlled Interfacial Interactions. *Macromolecules* **2009**, *42*, 4896–4901.
- Son, J. G.; Bulliard, X.; Kang, H. M.; Nealey, P. F.; Char, K. Surfactant-Assisted Orientation of Thin Diblock Copolymer Films. *Adv. Mater.* **2008**, *20*, 3643–+.
- Cloupeau, M.; Prunetfoch, B. Electrostatic Spraying of Liquids in Cone-Jet Mode. *J. Electrostat.* **1989**, *22*, 135–159.
- Jaworek, A. Micro- and Nanoparticle Production by Electrospraying. *Powder Technol.* **2007**, *176*, 18–35.
- Jaworek, A. Electrospray Droplet Sources for Thin Film Deposition. *J. Mater. Sci.* **2007**, *42*, 266–297.
- Chen, D. R.; Pui, D. Y. H.; Kaufman, S. L. Electrospraying of Conducting Liquids for Monodisperse Aerosol Generation in the 4 nm to 1.8  $\mu$ m Diameter Range. *J. Aerosol. Sci.* **1995**, *26*, 963–977.
- Rosellompart, J.; Delamora, J. F. Generation of Monodisperse Droplets 0.3 to 4  $\mu$ m in Diameter from Electrified Cone-Jets of Highly Conducting and Viscous-Liquids. *J. Aerosol. Sci.* **1994**, *25*, 1093–1119.
- Chen, D. R.; Pui, D. Y. H. Experimental Investigation of Scaling Laws for Electrospraying: Dielectric Constant Effect. *Aerosol Sci. Technol.* **1997**, *27*, 367–380.
- Ganan-Calvo, A. M.; Davila, J.; Barrero, A. Current and Droplet Size in the Electrospraying of Liquids. Scaling Laws. *J. Aerosol. Sci.* **1997**, *28*, 249–275.
- Gomez, A.; Tang, K. Q. Charge and Fission of Droplets in Electrostatic Sprays. *Phys. Fluids* **1994**, *6*, 404–414.
- Tang, K.; Gomez, A. On the Structure of an Electrostatic Spray of Monodisperse Droplets. *Phys. Fluids* **1994**, *6*, 2317–2332.
- Rietveld, I. B.; Kobayashi, K.; Yamada, H.; Matsushige, K. Morphology Control of Poly(vinylidene fluoride) Thin Film Made with Electrospray. *J. Colloid Interface Sci.* **2006**, *298*, 639–651.
- Rietveld, I. B.; Kobayashi, K.; Yamada, H.; Matsushige, K. Electrospray Deposition Producing Ultra-thin Polymer Films with a Regular Surface Structure. *Soft Matter* **2009**, *5*, 593–598.
- Rietveld, I. B.; Kobayashi, K.; Yamada, H.; Matsushige, K. Electrospray Deposition, Model, and Experiment: Toward General Control of Film Morphology. *J. Phys. Chem. B* **2006**, *110*, 23351–23364.
- Luu, Y. K.; Kim, K.; Hsiao, B. S.; Chu, B.; Hadjigaryrou, M. Development of a Nanostructured DNA Delivery Scaffold via Electrospinning of PLGA and PLA-PEG Block Copolymers. *J. Controlled Release* **2003**, *89*, 341–353.
- Ma, M. L.; Hill, R. M.; Lowery, J. L.; Fridrikh, S. V.; Rutledge, G. C. Electrospun Poly(styrene-block-dimethylsiloxane) Block Copolymer Fibers Exhibiting Superhydrophobicity. *Langmuir* **2005**, *21*, 5549–5554.
- Ma, M. L.; Krikorian, V.; Yu, J. H.; Thomas, E. L.; Rutledge, G. C. Electrospun Polymer Nanofibers with Internal Periodic Structure Obtained by Microphase Separation of Cylindrically Confined Block Copolymers. *Nano Lett.* **2006**, *6*, 2969–2972.
- Rietveld, I. B.; Kobayashi, K.; Yamada, H.; Matsushige, K. Process Parameters for Fast Production of Ultra-thin Polymer Film with Electrospray Deposition under Ambient Conditions. *J. Colloid Interface Sci.* **2009**, *339*, 481–488.
- Kim, G.; Libera, M. Morphological Development in Solvent-Cast Polystyrene–Polybutadiene–Polystyrene (SBS) Triblock Copolymer Thin Films. *Macromolecules* **1998**, *31*, 2569–2577.
- Kim, S. H.; Misner, M. J.; Xu, T.; Kimura, M.; Russell, T. P. Highly Oriented and Ordered Arrays from Block Copolymers via Solvent Evaporation. *Adv. Mater.* **2004**, *16*, 226–231.
- Kim, S. H.; Misner, M. J.; Yang, L.; Gang, O.; Ocko, B. M.; Russell, T. P. Salt Complexation in Block Copolymer Thin Films. *Macromolecules* **2006**, *39*, 8473–8479.
- Young, W. S.; Epps, T. H. Salt Doping in PEO-Containing Block Copolymers: Counterion and Concentration Effects. *Macromolecules* **2009**, *42*, 2672–2678.

44. Wang, J. Y.; Chen, W.; Roy, C.; Sievert, J. D.; Russell, T. P. Influence of Ionic Complexes on Phase Behavior of Polystyrene-*b*-poly(methyl methacrylate) Copolymers. *Macromolecules* **2008**, *41*, 963–969.

45. Epps, T. H.; Bailey, T. S.; Waletzko, R.; Bates, F. S. Phase Behavior and Block Sequence Effects in Lithium Perchlorate-Doped Poly(isoprene-*b*-styrene-*b*-ethylene oxide) and Poly(styrene-*b*-isoprene-*b*-ethylene oxide) Tri-block Copolymers. *Macromolecules* **2003**, *36*, 2873–2881.

46. Almeria, B.; Deng, W. W.; Fahmy, T. M.; Gomez, A. Controlling the Morphology of Electrospray-Generated PLGA Microparticles for Drug Delivery. *J. Colloid Interface Sci.* **2010**, *343*, 125–133.

47. Hogan, C. J.; Yun, K. M.; Chen, D. R.; Lenggoro, I. W.; Biswas, P.; Okuyama, K. Controlled Size Polymer Particle Production via Electrohydrodynamic Atomization. *Colloids Surf., A* **2007**, *311*, 67–76.

48. Bang, J.; Jeong, U.; Ryu, D. Y.; Russell, T. P.; Hawker, C. J. Block Copolymer Nanolithography: Translation of Molecular Level Control to Nanoscale Patterns. *Adv. Mater.* **2009**, *21*, 4769–4792.

49. Kim, S.; Briber, R. M.; Karim, A.; Jones, R. L.; Kim, H. C. Environment-Controlled Spin Coating to Rapidly Orient Microdomains in Thin Block Copolymer Films. *Macromolecules* **2007**, *40*, 4102–4105.

50. Peters, R. D.; Yang, X. M.; Kim, T. K.; Sohn, B. H.; Nealey, P. F. Using Self-Assembled Monolayers Exposed to X-rays to Control the Wetting Behavior of Thin Films of Diblock Copolymers. *Langmuir* **2000**, *16*, 4625–4631.

51. Han, E.; Gopalan, P. Cross-Linked Random Copolymer Mats as Ultrathin Nonpreferential Layers for Block Copolymer Self-Assembly. *Langmuir* **2010**, *26*, 1311–1315.

52. Han, S.; Shin, C.; Kim, E.; Ryu, D. Y.; Jeong, U.; Russell, T. P.; Hawker, C. J. Microdomain Orientation of PS-*b*-PMMA by Controlled Interfacial Interactions. *Macromolecules* **2008**, *41*, 6431–6437.

53. Esswein, B.; Moller, M. Polymerization of Ethylene Oxide with Alkyllithium Compounds and the Phosphazene Base “*t*-BuP<sub>4</sub>”. *Angew. Chem.* **1996**, *35*, 623–625.

54. Forster, S.; Kramer, E. Synthesis of PB-PEO and PI-PEO Block Copolymers with Alkyllithium Initiators and the Phosphazene Base *t*-BuP<sub>4</sub>. *Macromolecules* **1999**, *32*, 2783–2785.

55. Deng, W. W.; Klemic, J. F.; Li, X. H.; Reed, M. A.; Gomez, A. Increase of Electrospray Throughput Using Multiplexed Microfabricated Sources for the Scalable Generation of Monodisperse Droplets. *J. Aerosol. Sci.* **2006**, *37*, 696–714.

56. Deng, W. W.; Waits, C. M.; Morgan, B.; Gomez, A. Compact Multiplexing of Monodisperse Electrosprays. *J. Aerosol. Sci.* **2009**, *40*, 907–918.